Contents list available at CBIORE journal website

International Journal of Renewable Energy Development

Journal homepage: https://ijred.cbiore.id

Research Article

Advanced one-dimensional heterogeneous model for high temperature water gas shift membrane reactors

Wail El Bazi [a*], Abderrahim El-Abidi [b], Said Yadir[b], Brahim Messnaoui[b]

[a]*Laboratory of Process Engineering, Computer Science and Mathematics, Department of Process Engineering (LIPIM), National School of Applied Sciences of Khouribga, Sultan Moulay Slimane University, Bd Béni Amir, BP 77, 25000, Khouribga, Morocco.*

[b]*Laboratory of Materials, Processes, Environment and Quality (LMPEQ), National School of Applied Sciences of Safi, Cadi Ayyad University, Route Sidi Bouzid BP 63, 46000 Safi, Morocco.*

Abstract. To predict the behavior of small-scale WGS membrane reactors, a new model based on the 1D heterogeneous approach was developed. Unlike most studies, which rely on 1D pseudo-homogeneous models—typically limited to reactors filled with small catalyst particles which are prone to misestimating catalytic effectiveness when larger catalyst grains are used in which mass transfer resistance is usually considered only within the dense membrane layer which a valid assumption only when this layer is thick, the proposed model adapts to a wide range of catalyst sizes and geometries and also accounts for resistance in the porous stainless steel support of the membrane. This makes it suitable when the dense layer is thin. Comparison with experimental data under various conditions validated the model's ability to predict the behavior of reactors packed with large catalyst particles (V_{grain} ≈ 169 mm³). Therefore, the developed 1D heterogeneous model accurately predicts membrane reactor behavior without resorting to more complex 2D models. Simulations highlighted the significant influence of particle geometry on the catalyst effectiveness factor throughout the reactor, while its impact on carbon monoxide conversion, hydrogen partial pressure, and the temperature profile is especially pronounced near the reactor inlet. Additionally, results showed that sweep gas use accelerates the reaction and aids hydrogen permeation. Finally, CO conversion in the membrane reactor reached 1.3 times that of a conventional fixed-bed reactor.

Keywords: Catalyst geometry, effectiveness factor**,** membrane reactor, permeate zone, sweep gas.

Received: 17th March 2025; Revised: 15th June 2025; Accepted: 10th July 2005; Available online: 15th July 2025

1. Introduction

Hydrogen production has attracted increasing attention due to its vital role as a clean energy carrier and its applications in fuel cell technology (Adrover *et al.*, 2009a; Marin *et al.*, 2012). Beyond its energy applications, hydrogen is also a key component in various industrial processes, including ammonia production (El Bazi *et al.*, 2022; Gao *et al.*, 2019), methanol synthesis, Fischer-Tropsch processes, and steam gasification (El Bazi *et al.*, 2022). Industrially, hydrogen is predominantly produced via the Water Gas Shift (WGS) reaction, in which carbon monoxide reacts with water vapor to generate valuable hydrogen and carbon dioxide, following the chemical equation below (Boutikos & Nikolakis, 2010):

$$CO + H_2O \rightleftarrows CO_2 + H_2 \quad (1) \qquad \Delta H_R(298K) = -41.2 \text{ kJ mol}^{-1}$$

This reversible exothermic reaction is thermodynamically limited at high temperatures (Gosiewski *et al.*, 2010). One approach to overcoming this limitation is the use of membrane reactors that selectively permeate either hydrogen or carbon dioxide. Hydrogen-permeable membranes are typically made of palladium, though other materials such as silica, zeolite, carbon, and polymers have also been investigated (Gao *et al.*, 2019). Alternatively, carbon dioxide can be selectively removed using ceramic carbonate membranes (Eddi & Chibane, 2020; Huang *et al.*, 2022) or silicate-based membranes (Wirawan *et al.*, 2012). By continuously separating hydrogen or carbon dioxide from the reaction mixture, the membrane reactor shifts the equilibrium toward product formation, thereby enhancing carbon monoxide conversion (Eddi & Chibane, 2020). This enhancement results from a decrease in CO_2 and H_2 concentrations, which favors the WGS reaction rate within the reactor (Eddi & Chibane, 2020; Sanz *et al.*, 2015).

Numerous experimental studies (Augustine *et al.*, 2011; Basile *et al.*, 2015; Mendes *et al.*, 2011; Sanz *et al.*, 2013; Sanz *et al.*, 2014; Sanz *et al.*, 2015) have shown that this technology surpasses conventional fixed-bed reactors in terms of hydrogen purification and carbon monoxide removal (Sanz *et al.*, 2014; Sanz *et al.*, 2015). Moreover, it has been shown that the efficiency of this process depends on several parameters, including pressure, temperature, the H_2O/CO molar ratio, the reactor feed flow rate, and the sweep gas flow rate (Basile et al., 2015; Sanz *et al.*, 2014; Sanz *et al.*, 2015).

In this technology, the WGS reaction takes place within a fixed-bed reactor packed with a catalyst. The reactor wall is typically a composite membrane composed of multiple layers (Adrover., 2009b; Israni & Harold, 2011; Marin *et al.*, 2012; Sanz

* Corresponding author
Email: w.elbaziil@usms.ma (W. El Bazi)

https://doi.org/10.61435/ijred.2025.61222
ISSN: 2252-4940/© 2025.The Author(s). Published by CBIORE

et al., 2013; Sanz et al., 2015; Wirawan *et al.*, 2012). For instance, Pd-based membranes (Sanz *et al.*, 2013) generally feature two distinct layers:

- A porous layer made of stainless steel and Fe-Cr oxide, which is in direct contact with the reaction mixture.
- A dense second layer, primarily composed of palladium, covering the first one.

Hydrogen permeates through these layers and is collected as permeate, whereas other components remain in the retentate. The sweep gas flows through the permeate side, enhancing hydrogen flux through the membrane by reducing the H_2 concentration. This reduction lowers the partial pressure on the permeate side, thereby increasing the driving force for hydrogen permeation (Basile *et al.*, 2015). The most commonly used sweep gases are nitrogen and air (Huang., 2005).

The reactor is primarily packed with two types of catalysts:

- Low-temperature catalysts (200–300°C), typically based on copper oxide (Brunetti., 2007).
- High-temperature catalysts (300–500°C), primarily based on iron oxide (Marin *et al.*, 2012).

Modeling and simulating membrane reactors (MRs) remain essential tool for predicting their behavior, optimizing their operation, and guiding their design**.** The models used can be classified into two categories: One-dimensional (1D) and multidimensional (2D, 3D) models.

1D models:

- 1D pseudo-homogeneous reactor-side models: These models do not account for mass and heat transfer resistances inside or around the catalytic particles and assume plug flow in the reactor. This approach is the most widely used in the literature (Adrover *et al.*, 2009a; Adrover *et al.*, 2017; Alihellal & Chibane, 2019; Alihellal *et al.*, 2024; Bishop & *Lima*, 2020; Boutikos & Nikolakis, 2010; Coronel *et al.*, 2011; Eddi & Chibane, 2020; Makertiharta *et al.*, 2017; Radcliffe *et al.*, 2016) due to its mathematical simplicity compared to other models. However, for large catalyst grain sizes, mass and heat transfer limitations become significant, and neglecting them can lead to inaccuracies.
- 1D heterogeneous models on the reactor side: This approach is less common for modeling WGS membrane reactors (Brunetti *et al.*, 2007; Karagoz *et al.*, 2018; Karagoz *et al.*, 2020). These models account for transfer limitations and are more suitable for approximating experimental results when catalyst grain diameters are large (Karagoz *et al.*, 2018). They predict intra-granular concentrations, temperatures, and reaction rates (Karagoz *et al.*, 2018; Karagoz *et al.*, 2020) and provide a better assessment of the impact of grain size on MRs (Karagoz *et al.*, 2018). These models assume plug flow and adjust reaction rates using an effectiveness factor estimated from inter- and intra-granular reaction kinetics. Some researchers, such as Brunetti *et al.* (2007) have used the Thiele approach to estimate this factor, while Karagöz *et al.* (2018) & (2020) employed methods such as the Dusty Gas Model (DGM), the Stefan-Maxwell Model (SMM), and the Wilke Model (WM).

1D models remain acceptable for predicting the behavior of laboratory-scale reactors with a small diameter (Adrover., 2009b; Huang., 2005; Radcliffe., 2016). Moreover, several studies have demonstrated that these models can accurately predict experimental results for this type of membrane reactor (Coronel *et al.*, 2011; Garshasbi *et al.*, 2019; Ma & Lund, 2003; Mendes *et al.*, 2011; Oyama & Hacarlioglu, 2009). However, when the reactor diameter is large, it is advisable to adopt multidimensional models to account for radial or even angular dispersion, which is further intensified by membrane permeation. Multidimensional models can be classified as follows:

- 2D pseudo-homogeneous models account for axial and radial dispersion while neglecting intra- and inter-particle transfer resistances. Radial velocity and concentration variations are significant in MRs due to mass and heat permeation through the membrane (Marin *et al.*, 2012; Sanz *et al.*, 2015). While mathematically complex, these models are widely used (Lundin *et al.*, 2023; Markatos *et al.*, 2005; Oyama & *Hacarlioglu*, 2009; Piemonte *et al.*, 2015) and provide accurate predictions for reactors packed with small catalyst particles ($d_p \ll 1$ mm) (Oyama & Hacarlioglu, 2009).
- 2D heterogeneous models account for axial and radial dispersion, as well as intra- and inter-particle transfer resistances. Although less commonly used (Marin *et al.*, 2012; Sanz *et al.*, 2015) due to their mathematical complexity, they offer more accurate predictions for reactors with large catalyst particles ($d_p \gg 1$ mm) (Sanz *et al.*, 2015).
- 3D reactor models provide the most comprehensive approach, capturing the entire reactor geometry and predicting profiles in angular directions, making them particularly suitable for modeling asymmetric converters (Marin *et al.*, 2012). These models have been shown to match experimental data accurately (Chein *et al.*, 2014).

Diffusion through the dense layer is the rate-limiting step in membrane permeation (Chein et al., 2014; Coronel., 2011), which is why most studies consider only this step when estimating the permeate flux (Adrover et al., 2009a; Adrover et al., 2017; Brunetti., 2007; Chein et al., 2014; Eddi & Chibane, 2020; Gosiewski et al., 2010; Karagoz et al., 2018; Ma & Lund, 2003; Marin et al., 2012; Smith et al., 2011). However, some studies also account for the resistance of the porous support layer, particularly when the dense layer is thin and the permeate flux is high (Sanz et al., 2013; Sanz et al., 2015).

This review of 1D and multidimensional MR models reveals that few studies have developed MR models incorporating intra-particle transfer resistances. Moreover, most existing models estimate the permeate flux based solely on the resistance of the dense layer. However, for reactors packed with large catalyst grains ($d_p > 1$ mm) and/or equipped with thin dense-layer membranes, a model that accounts for both the catalytic grain effectiveness factor and all major mass transfer resistances within the membrane is necessary. Although multidimensional models can account for dispersive transport phenomena, they remain mathematically complex and computationally demanding, and may not be necessary for laboratory-scale reactors where radial gradients are often negligible due to the small reactor diameter. Therefore, it is of great interest to develop a 1D model that integrates both inter- and intra-particle diffusion limitations as well as the mass transfer resistances associated with the various layers of the membrane, without resorting to a multidimensional approach, especially when the reactor diameter is small. This highlights a gap in the literature and provides a

strong rationale for developing a new 1D model that is both accurate and easier to implement numerically for configurations involving large catalyst grains, thin dense-layer membranes, and small-scale membrane reactors.

In this study, we developed a novel 1D model to predict the behavior of small-scale WGS membrane reactors while incorporating key transfer phenomena. Unlike other MR modeling studies that employed various heterogeneous approaches (Brunetti *et al.*, 2007; Karagoz *et al.*, 2018; Karagoz *et al.*, 2020; Marin *et al.*, 2012; Sanz *et al.*, 2015), we employed the rigorous heterogeneous approach to estimate the catalytic effectiveness factor. We also consider both palladium layer diffusion and stainless-steel porous support diffusion when estimating permeate flux, unlike most studies that focus solely on the dense layer.

First, we compared our model's results with those of the 1D pseudo-homogeneous model and with experimental and simulation data from the literature (Sanz *et al.*, 2014; Sanz *et al.*, 2015). Next, the rigorous heterogeneous model was employed to analyze the impact of catalyst geometry and sweep gas flow rate on reactor behavior. Finally, we compared the performance of the membrane reactor with that of a conventional fixed-bed reactor.

2. Methods

In the Methods section, we first describe the initial and operating conditions as well as the process characteristics considered in the simulations, providing justification for their selection. This is followed by a detailed presentation of the adopted membrane reactor modeling approach and the corresponding governing equations.

2.1 *Description of the Characteristics and Operating Conditions of the Processes Considered in the Simulation*

The initial simulations aim to determine which of the two models developed in this study best aligns with experimental data, and to evaluate these models against the more comprehensive and mathematically complex 2D heterogeneous approach. Therefore, the results obtained from these models were compared with those from experimental and modeling studies available in the literature (Sanz *et al.*, 2014; Sanz *et al.*, 2015).

The feed composition, operating conditions, membrane reactor characteristics, and catalyst properties (composition, density, volume, shape, and intragranular characteristics) considered in the simulation correspond to those described in the studies (Sanz *et al.*, 2014; Sanz *et al.*, 2015). The model results were assessed by comparing the experimental CO conversion with the CO conversion predicted by the models.

The statistical indicators used for this comparison are the Absolute Relative Error (ARE) and the Mean Absolute Relative Error (MARE), expressed by the following equation:

$$Mare = \frac{1}{n_P}\sum_{i=1}^{n_P}\left|\frac{X_{CO,mod}-X_{CO,exp}}{X_{CO,exp}}\right| = \frac{1}{n_P}\sum_{i=1}^{n_P} ARE \quad (2)$$

where n_P is the number of experiments, $X_{CO,mod}$ is the model-predicted CO conversion, and $X_{CO,exp}$ is the experimental CO conversion.

In the second part of the simulations, a sensitivity analysis was performed on the rigorous 1D heterogeneous model developed in this work. The studied process corresponds to an isoperibolic shell-and-tube system, in which the permeate and sweep gases flow inside the tube, while the reaction zone is located in the annulus side packed with catalyst. The tube consists of a multilayer membrane that includes a porous stainless-steel layer in direct contact with the reaction mixture, followed by a palladium layer covering it. The shell is maintained at a constant temperature, T_{Sh}.

The characteristics of the membrane reactor, the catalyst, and the operating conditions used in the simulation are presented in Table 1, whereas the process scheme corresponding to this section, including a schematic representation of the main mass transfer, heat transfer, and

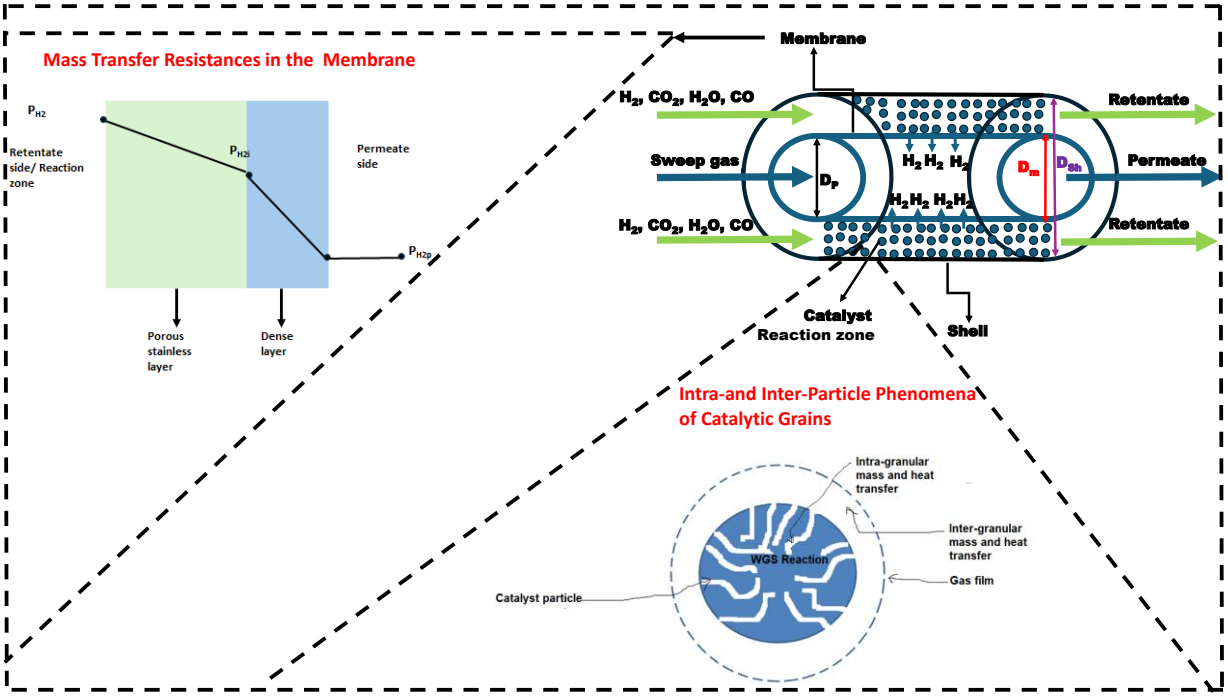

Fig. 1 Process schematic with main phenomena in membrane and catalyst grain

Table 1
Characteristics of the membrane reactor, catalyst, and operating conditions considered in the simulation

Molar feed composition	Dry basis: 70% H_2-18% CO-12% CO_2 H_2O/CO=1
Membrane reactor characteristics	Reaction zone: Reactor length: L=25 cm Shell diameter: D_{Sh}=2.27 cm Shell temperature: T_{Sh}=623.15 K Membrane: Porous stainless support and Dense layer of Pd with e_{Pd} =10.2 µm External diameter of tube: D_m=0.9 cm, Internal diameter of tube (permeate zone): D_p= 0.51 cm
Catalyst composition and density	Fe_3O_4-Cr_2O_3-1960 kg.m^{-3}
Intragranular catalyst properties	[1]
Permeate pressure (P_P)	1 atm
Transmembrane pressure (ΔP)	2 bars
Total molar flow (F_T)	0.0308 mol.min^{-1}
Feed temperature	623.15 K
Catalyst shape and volume	Cylinder-Sphere / 169 mm^3- 44.6 mm^3 -0.52 mm^3
Heat transfer mode	Isoperibolic
Molar flow of sweep gas (N_2)	0 ml.s^{-1} - 6.72 ml.s^{-1}- 20 ml.s^{-1}

chemical reaction phenomena occurring in the catalytic grain and in the membrane, is shown in Figure 1.

The composition of the syngas corresponds to the outlet streams of methane reforming reactors or biomass gasifiers (Sanz *et al*., 2014; Sanz *et al*., 2015). The operating temperature falls within the range of experimental conditions used during the development of the kinetic equation for the water-gas shift (WGS) reaction in the presence of the selected catalyst (Keiski *et al*., 1993).

The membrane considered in the simulation is similar to the one studied in experimental works (Sanz *et al*., 2014; Sanz *et al*., 2015), with permeation characteristics available in the literature (Sanz *et al*., 2013). The length and diameter of the setup fall within the range of laboratory-scale membrane reactors (Garshasbi *et al*., 2019; Karagoz *et al*., 2018; Mendes *et al*., 2011; Sanz *et al*., 2014; Sanz *et al*., 2015). A relatively long laboratory reactor was chosen to enable the visualization of pressure losses along the reactor and temperature profiles in the case of a non-isothermal reactor. Indeed, a reactor with a short length would not provide adequate visualization of the evolution of these parameters along the system.

2.2 Membrane Reactor Modeling

The adoption of a 1D modeling approach is further supported by the small diameter of the membrane reactors considered in this study, which limits radial gradients in temperature and concentration (Adrover, 2009b; Huang, 2005; Radcliffe, 2016). This assumption has proven to be valid, as several laboratory-scale studies have shown that 1D models can provide results in good agreement with experimental data (Coronel *et al*., 2011; Garshasbi *et al*., 2019; Ma & Lund, 2003; Mendes *et al*., 2011; Oyama & Hacarlioglu, 2009).

The computational code for numerically solving the equations presented in this section was developed in MATLAB.

2.2.1. Reactor Modeling

2.2.1.1. One-Dimensional Heterogeneous Model

The studied reactor is a fixed-bed reactor packed with a Fe_3O_4-Cr_2O_3-based catalyst, whose characteristics are provided in (Sanz *et al*., 2015). The membrane forming the reactor wall is selectively permeable to hydrogen. The system is fed with a mixture of CO, CO_2, H_2, and H_2O. The mass balance results in the following ordinary differential equations (Eddi & Chibane, 2020):

The reactants (CO, H_2O) are impermeable to the membrane. Therefore, for these species:

$$\frac{dF_i}{dz} = \eta_e \cdot F_{Pres} \cdot r_{CO}\, \rho_B \cdot S_R \quad (3)$$

For CO_2 (impermeable to the membrane):

$$\frac{dF_{CO2}}{dz} = -\eta_e \cdot F_{Pres} \cdot r_{CO}\, \rho_B \cdot S_R \quad (4)$$

To calculate the hydrogen molar flow rate inside the reactor, considering the hydrogen mole flow rate leaving through the permeate, the mass balance is given by the following equation:

$$\frac{dF_{H2}}{dz} = -\eta_e \cdot F_{Pres} \cdot r_{CO}\, \rho_B \cdot S_R - \pi D_m J_{H2} \quad (5)$$

The hydrogen molar flow rate in the permeate along the membrane ($\pi D_m J_{H2}$) is also expressed by the following differential equation:

$$\frac{dF_{H2,p}}{dz} = \pi D_m J_{H2} \quad (6)$$

The intrinsic reaction rate of the WGS, $-r_{CO}$ (mol.kg^{-1}.s^{-1}), is expressed as a function of reactants and products concentrations, as well as the equilibrium constant, through the following equation:

$$-r_{CO} = 3714.5\, exp\left(\frac{-66578.512}{R_g T}\right) {C_{CO}}^{0.54} {C_{H2O}}^{0.1} [1 - \beta] \quad (7)$$

With: $\beta = \frac{C_{CO2} C_{H2}}{C_{CO} C_{H2O}} \frac{1}{K_e}$ and : $K_e = exp\left(\frac{4577.8}{T} - 4.33\right)$ (8)

where: η_e is the overall effectiveness factor, F_{pres} is the pressure scale-up factor (calculation in (El Bazi *et al*., 2022)), ρ_B is the bed density (kg.m^{-3}) (formula available in (El Bazi *et al*., 2022)), S_R is the reactor cross-sectional area (m^2), given by $\pi . r_m^2$ for a simple membrane reactor and $\pi . r_{Sh}^2 - \pi . r_m^2$ for a shell-and-tube system,

r_m is the reactor radius (m), r_{Sh} is the shell radius (m), J_{H2} is the permeation flow of H_2 (mol. $s^{-1}.m^{-2}$), R_g is the ideal gas constant (8.314 $J.mol^{-1}.K^{-1}$), C_i is the concentration of species i ($mol.m^{-3}$), and K_e is the equilibrium constant.

To evaluate the pressure drop ΔP (Pa) along the membrane reactor, several studies adopt the Ergun equation (Alihellal & Chibane, 2016a; Alihellal & Chibane, 2016b; Bishop & *Lima*, 2020):

$$\frac{dP}{dz} = -\frac{1-\varepsilon_B}{{\varepsilon_B}^3}\left(\mathbf{1.75} + \mathbf{150}\frac{1-\varepsilon_B}{Re}\right)\frac{\rho u_s^2}{d_p} \quad (9)$$

where: ε_B is the bed porosity, Re is the Reynolds number (El Bazi et al., 2022), ρ is the gas density ($kg.m^{-3}$) (El Bazi *et al*., 2022), u_s is the superficial gas velocity (m. s^{-1}) (El Bazi *et al*., 2022), and d_p is the equivalent particle diameter (m).

For a tube-and-shell isoperibolic membrane reactor, the heat balance in the reaction zone considers the heat flux released by the chemical reaction, the convective heat exchanges between the shell and the reaction medium, between the membrane wall and this medium, as well as the heat flux evacuated through the permeate. This leads to the following differential equation (Meng *et al*., 2021):

$$\sum \boldsymbol{F_i C_{pi}}\frac{dT}{dZ} = \eta_{\boldsymbol{e}}\boldsymbol{\Delta H_R . F_{Pres} r_{CO} . \rho_B .\ S_R\ } - \boldsymbol{\pi . D_{Sh} . h_{int}(T - T_{Sh}) - J_{H2} . \pi . D_m . C_{p,H2} . (T - T_P) - U_m . \pi . D_m . (T - T_P)} \quad (10)$$

In the permeate zone (containing either hydrogen alone in the absence of sweep gas, or nitrogen and hydrogen in the presence of sweep gas), the heat balance considers the heat flux associated with the hydrogen feeding this zone and the convective heat exchange between the membrane wall and the gas mixture flowing through the permeate zone, which leads to the following differential equation (Meng *et al*., 2021):

$$\boldsymbol{\left(F_{H2,P} C_{p\,H2} + F_S C_{p\,N2}\right).\frac{dT_P}{dZ} = J_{H2} . \pi . D_m . C_{p,H2}(T - T_P) + U_m . \pi . D_m . (T - T_P)} \quad (11)$$

where: F_i is the molar flow rate of component i in the reaction zone (mol. s^{-1}), $C_{p,i}$ is the molar heat capacity of component i ($J.mol^{-1}.K^{-1}$) (El Bazi *et al*., 2022), T is the temperature in the reaction zone (K), ΔH_R is the reaction heat for WGS ($J.mol^{-1}$), h_{int} is the individual heat transfer coefficient for packed bed reactor side (W. $m^{-2}.K^{-1}$), T_{Sh} is the shell temperature (K), U_m is the overall heat transfer coefficient between the permeate and the reaction zone (W. $m^{-2}.K^{-1}$), T_P is the permeate zone temperature (K), F_S is the molar flow rate of the sweep gas (mol. s^{-1}).

The expression for ΔH_R is given in (El Bazi *et al*., 2022), while the estimation method for h_{int} can be found in (El Bazi *et al*., 2023). The overall heat transfer coefficient is calculated using:

$$\boldsymbol{U_m} = \frac{\mathbf{1}}{\boldsymbol{h_{int}}} + \frac{\boldsymbol{D_m}}{\boldsymbol{D_P}}.\frac{\mathbf{1}}{\boldsymbol{h_P}} \quad (12)$$

where h_P denotes the convective heat transfer coefficient in the permeate (W. $m^{-2}.K^{-1}$) (Olatunji *et al*., 2018).

The molar flow rates, temperatures, and pressure are well known at Z=0 (Table 1), so the system of ordinary differential equations (3-6 and 9-11) is solved using the fourth-order Runge-Kutta method. For a conventional fixed-bed reactor, J_{H2}=0, and all equations are considered except (6) and (11). For Equation (10), heat transfer terms between the reactor and the permeate are not considered for this technology.

2.2.1.2. 1D Pseudo-Homogeneous Model

The equations of this model are similar to those of the 1D heterogeneous model; however, in this case, we assume η_e = 1. Indeed, mass and heat transfer limitations between the catalyst and the gas flowing through the reactor are neglected in this approach.

2.2.2. Membrane Modeling

Mass transport through the membrane can be described by considering two main resistances to mass transfer (Sanz *et al*., 2013), as illustrated in Figure 1

The first is associated with the porous stainless-steel layer. In this region, the permeation flux of hydrogen (J_{H2}) is expressed as a function of temperature and the partial pressure difference across the layer:

$$\boldsymbol{J_{H2} = 2.8.10^{-5} T^{-0.5}.(mol.s^{-1}m^{-2}.Pa).(P_{H2} - \ P_{H2i}\ )} \quad (13)$$

The second resistance corresponds to the palladium layer, where hydrogen permeation follows Sievert's law. The hydrogen flux is given by:

$$\boldsymbol{J_{H2} = exp\left(-3.19 - \frac{2803}{T}\right).(mol.s^{-1}m^{-2}.Pa^{-0.5}).(P_{H2i}^{0.5} - P_{H2p}^{0.5}\ )} \quad (14)$$

where P_{H2} and P_{H2i} correspond to the partial pressure of hydrogen in the reaction zone (Pa) and at the interface between the porous stainless steel (PSS) layer and the palladium (Pd) layer, respectively. The partial pressure of hydrogen in the reaction zone (P_{H_2}) is determined using Dalton's law:

$$\boldsymbol{P_{H2} = \frac{F_{H2}}{\sum F_i}.P} \quad (15)$$

In the absence of a sweep gas, the hydrogen pressure in the permeate equals the permeate pressure Pp (Pa). When a sweep gas with a molar flow rate F_S ($mol{\cdot}s^{-1}$) is present, the hydrogen partial pressure in the permeate (P_{H2p}) is calculated using Dalton's law (Alihellal & Chibane, 2016b):

$$\boldsymbol{P_{H2p} = \frac{F_{H2,p}}{F_{H2,p}+F_S}.P_p} \quad (16)$$

2.2.3. Catalyst particle model and Estimation of η_e for the Rigorous Heterogeneous Model

The modeling of the catalytic grain focuses on the inter- and intra-particle phenomena presented in Figure 1.

The establishment of the intragranular mass balance leads to differential equations with boundary condition problems as follows (El Bazi *et al*., 2023):

For Reactants:

$$\boldsymbol{D_{e,i}\frac{1}{r^q}\frac{d}{dr}\left(r^q\frac{dC_i}{dr}\right) + \rho_c F_{Pres} r_{CO}(r) = 0} \quad (17)$$

For Products:

$$\boldsymbol{D_{e,i}\frac{1}{r^q}\frac{d}{dr}\left(r^q\frac{dC_i}{dr}\right) - \rho_c F_{Pres} r_{CO}(r) = 0} \quad (18)$$

where: $D_{e,i}$ is the effective diffusive coefficient of the species i, calculated based on Knudsen diffusivity ($m^2.s^{-1}$) (El Bazi *et al*., 2022), r represents the intraparticle spatial position (m). For

cylinders or spheres, r varies between 0 and the radius, the factor q is equal to 1 for a cylinder and 2 for a sphere, ρ_c is the catalyst density (kg.m^{-3}) and $r_{CO}(r)$ is the reaction rate at the position r.

At the center of the particle (r=0), the reactants concentrations are minimal, while the product concentrations are maximal, leading to the following condition:

$$\frac{dC_i}{dr}(\boldsymbol{r = 0}) = \boldsymbol{0} \quad (19)$$

The catalytic particle is surrounded by a gas film, where mass and heat transfer occur between the catalyst surface and the bulk gas (figure 1). The mass flux exchanged between the bulk gas and the catalyst surface is expressed as:

$$K_{C,i}(C_{i,f} - C_{i,s}) = D_{e,i}\frac{dC_i}{dr}(r = R) \quad (20)$$

The energy balance around the particle leads to the following equations:

For Reactants:

$$h(T_s - T_f) = -D_{e,i}\frac{dC_i}{dr}(r = R)\ )\Delta H_r \quad (21)$$

For Products:

$$h(T_s - T_f) = D_{e,i}\frac{dC_i}{dr}(r = R\ )\Delta H_r \quad (22)$$

where: $K_{C,i}$ is the mass transfer coefficient of species i (m.s^{-1}), with its calculation formula provided in (El Bazi *et al.*, 2022), $C_{i,f}$ is the molar concentration of species i in the bulk gas (mol.m^{-3}), $C_{i,s}$ is the molar concentration of species i at the particle surface (mol.m^{-3}), h is the heat transfer coefficient between the particle surface and the bulk gas (W. m^{-2}.K^{-1}) (El Bazi *et al.*, 2022), T_s and T_f are the temperatures at the particle surface and the bulk gas (K), respectively, R is the radius of the catalytic particle (m).

The particle is considered isothermal (El Bazi *et al.*, 2023) if:

$$\left|\frac{\Delta H_R.D_{e,CO}.C_{CO,s}}{\lambda_e}\right| < 0.1 \quad (23)$$

where λe is the effective thermal conductivity of the particle (W. m^{-1}.K^{-1}) (El Bazi *et al.*, 2022).

For an isothermal particle, the concentrations and the temperature at the grain surface, as well as the intragranular concentrations of the chemical species involved in the WGS reaction, are obtained by numerically solving the system of differential equations (17-20) and (21) applied to CO. The numerical method used to solve this boundary value problem is the orthogonal collocation method, employing eight internal collocation points and two external collocation points, corresponding to the particle surface and center. This method is widely used for solving diffusion-reaction differential equations (El Bazi *et al.*, 2022; El Bazi *et al.*, 2023). The number of collocation points was determined based on previous studies (El Bazi *et al.*, 2022; El Bazi *et al.*, 2023).

The concentrations at the particle center, the concentrations and temperature at the particle surface, as well as the intragranular concentrations at various intragranular positions, are employed in equation 7 to estimate the reaction rates $-r_{CO}$ (r) at different collocation points. These reaction rates are subsequently employed to determine the overall effectiveness factor for various granular geometries (Villermaux., 1993):

For a Cylinder:

$$\eta_{\boldsymbol{e}} = \frac{1}{r_{CO,f}.V_p}\int_0^R .\boldsymbol{F_{Pres}}.\boldsymbol{r_{CO}}(\boldsymbol{r})\boldsymbol{L_C}.\boldsymbol{2}.\boldsymbol{\pi}.\boldsymbol{r}.\boldsymbol{dr} \quad (24)$$

For a Sphere:

$$\eta_{\boldsymbol{e}} = \frac{1}{r_{CO,f}.V_p}\int_0^R .\boldsymbol{F_{Pres}}.\boldsymbol{r_{CO}}(\boldsymbol{r}).\boldsymbol{4\pi r^2 dr} \quad (25)$$

where: $r_{CO,f}$ is the reaction rate in the bulk gas (mol. kg^{-1}. s^{-1}), V_p is the volume of the catalytic particle (m^3), L_C is the length of the cylindrical catalytic particle (m).

There exist other expressions of η_e adapted to different particle shapes, making the rigorous heterogeneous model applicable to various catalyst grain geometries (Villermaux., 1993).

3. Results and Discussion

3.1. Comparison of the Results of the Developed Models with Experimental and Simulated Data from the Literature: Effect of GSHV, T, H_2O/CO, and P on X_{CO}

Figures 2.a, 2.b, and 2.c compare the experimental data from the study (Sanz *et al.*, 2015), the predictions of the corresponding 2D heterogeneous model (2D het), and the results obtained using the models developed in the present study. These figures illustrate the effect of GSHV (gas-hourly space velocity measured at s.t.p., h^{-1}), temperature, and the H_2O/CO ratio on carbon monoxide conversion (X_{CO}). Figure 3 further investigates the influence of transmembrane pressure on X_{CO} by comparing the experimental data from the study (Sanz *et al.*, 2014) at different temperatures with the simulation results obtained using the models proposed in this work. Table 2 presents a summary table comparing the CO conversions (X_{CO}) obtained experimentally in the papers (Sanz *et al.*, 2014) and (Sanz *et al.*, 2015) with those obtained in the present study using the 1D heterogeneous model.

The results presented in these figures demonstrate a good agreement between the predictions of the rigorous 1D heterogeneous model (1D het) developed in this study and the experimental data from (Sanz *et al.*, 2014; Sanz *et al.*, 2015). In contrast, the 1D pseudo-homogeneous model (1D pseud-hom) significantly overestimates the experimental values. Specifically, the mean absolute relative error (MARE) for the 1D heterogeneous model in predicting the effect of GSHV on X_{CO} is 0.09, compared to 0.33 for the 1D pseudo-homogeneous model and 0.03 for the 2D model in (Sanz *et al.*, 2015). For the effect of temperature on X_{CO}, the MARE is 0.069 for the 1D heterogeneous model, 0.17 for the 1D pseudo-homogeneous model, and 0.082 for the 2D model in (Sanz *et al.*, 2015). Regarding the influence of the H_2O/CO ratio, the 1D heterogeneous model yields a MARE of 0.13, close to the 0.1 reported for the 2D model in (Sanz *et al.*, 2015), whereas the 1D pseudo-homogeneous model exhibits a much higher error of 0.41. Finally, for the effect of transmembrane pressure on X_{CO}, the MARE is 0.051 for the 1D heterogeneous model, compared to 0.15 for the 1D pseudo-homogeneous model. Overall, the maximum MARE for the 1D heterogeneous model remains below 13%, placing it in the same order of magnitude as the more computationally complex 2D heterogeneous model.

It is also observed that the 1D pseudo-homogeneous model is unreliable for predicting the behavior of a membrane reactor packed with large-diameter catalyst grains ($d_p \geq 6$ mm) (Sanz *et*

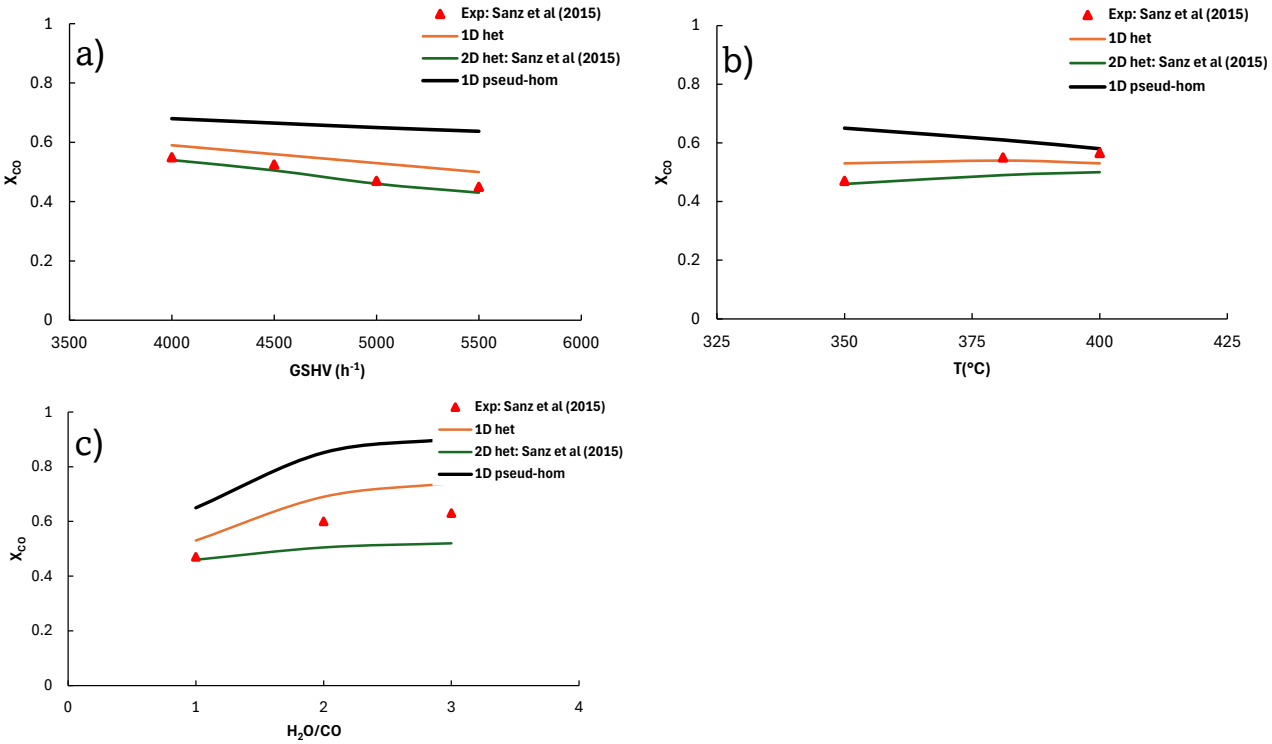

Fig. 2. Effect of operating conditions on X_{CO}: Comparison between experimental data (Sanz et al., 2015), 2D model results (Sanz et al., 2015), and 1D model results (this study). (a) Effect of GSHV (ΔP = 2 bars, T = 350°C, H_2O/CO = 1), (b) Effect of T (ΔP = 2 bars, GSHV = 5000 h^{-1}, H_2O/CO = 1), (c) Effect of H_2O/CO (ΔP = 2 bars, GSHV = 5000 h^{-1}, T = 350°C)

Table 2
Comparative table of CO conversion (X_{CO}): experimental results from Sanz et al. (2014–2015) vs. simulated results from the present study using the 1D rigorous heterogeneous model

Study	Parameter		X_{CO} Experimental	X_{CO} model	ARE	Mare
Sanz *et al.* 2014	ΔP/T (bars/°C)	2/350	0.47	0.53	0.12	0.051
		2/380	0.55	0.54	0.02	
		2/400	0.56	0.53	0.05	
		3/350	0.61	0.66	0.08	
		3/380	0.64	0.65	0.02	
		3/400	0.655	0.65	0.008	
Sanz *et al.* 2015	GHSV (h^{-1})	4000	0.55	0.59	0.07	0.09
		4500	0.525	0.56	0.06	
		5000	0.47	0.53	0.12	
		5500	0.45	0.5	0.11	
	Temperature	350	0.47	0.53	0.12	0.069
		381	0.55	0.54	0.02	
		400	0.565	0.53	0.06	
	H_2O/CO ratio	1	0.47	0.53	0.12	0.13
		2	0.6	0.68	0.13	
		3	0.63	0.72	0.14	

al., 2014; Sanz *et al.*, 2015). This model significantly overestimates X_{CO} values compared to experimental data, as it does not account for inter- and intra-granular mass transfer limitations, which slow down the reaction and consequently reduce reactant conversion. The lowest X_{CO} values are predicted by the 2D heterogeneous model. In addition to incorporating mass transfer resistances both around and within the catalyst particles, this model accounts for dispersive effects, which further slow the reaction and reduce X_{CO}.

The deviations observed in the heterogeneous models, while remaining within an acceptable range, can be attributed to several factors:

- Inaccurate prediction of dispersive phenomena.
- Imprecise estimation of intra-granular parameters or membrane permeability.
- Other potential sources of uncertainty in the model assumptions and experimental conditions.

Figure 2.a illustrates a decrease in X_{CO} with increasing GSHV. This trend can be attributed to the higher volumetric

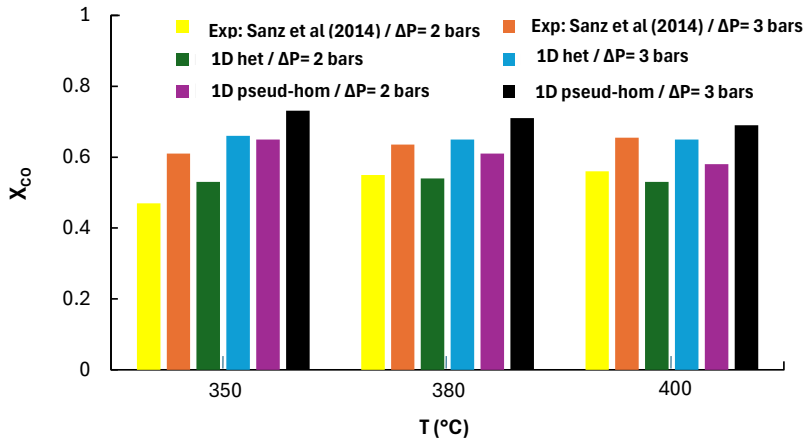

Fig. 3 Effect of ΔP on X_{CO} at different temperatures: Comparison of experimental results (Sanz *et al.*, 2014) and 1D model simulations (this study), with GHSV = 5000 h^{-1} and $H_2O/CO = 1$

feed rate at higher GSHV, which reduces the contact time between reactants and the catalyst, thereby lowering CO conversion. Based on the results in Figure 2.b, except for the curve corresponding to the 1D pseudo-homogeneous model, it can be observed that X_{CO} slightly increases with rising temperature. This slight increase in X_{CO} can be attributed to two opposing effects of temperature: on one hand, the increase in temperature enhances the kinetic constant and reactant concentrations, which favors an increase in the reaction rate. On the other hand, according to Le Chatelier's principle, to counteract the temperature rise, the thermodynamic equilibrium shifts in the direction of the reverse reaction, leading to a decrease in the thermodynamic equilibrium constant, K_e, as T increases. This, in turn, slows down the reaction rate and thus limits the increase in CO conversion. This limiting effect is less noticeable for the membrane (MR) compared to the conventional fixed-bed reactor (El Bazi *et al.*, 2022), due to the evacuation of hydrogen through the membrane, which leads to higher reaction rates.

For the 1D pseudo-homogeneous model, which does not account for inter- and intra-particle mass transfer resistances, the increase in temperature results in a slight reduction of X_{CO}. Under the assumptions of this model, the increases in the kinetic constant and reactant concentrations induced by the temperature rise are not sufficient to counterbalance the decrease in the equilibrium constant caused by this temperature increase. Except for the 2D heterogeneous model curve, Figure 2.c shows a significant increase in X_{CO} as the H_2O/CO ratio rises from 1 to 2, followed by a slight increase as the ratio increases from 2 to 3. The pronounced rise in X_{CO} in the first part of the curves is attributed to the higher H_2O concentration, which enhances the reaction rate (see Eq. 7). The subsequent slowdown in the X_{CO} increase is caused by a dilution effect due to the additional water. As the water concentration in the reaction zone increases, the CO concentration decreases, leading to a lower reaction rate. Furthermore, the reduction in hydrogen partial pressure resulting from this dilution decreases the H_2 permeation flow, hindering the equilibrium shift toward product formation. The increase in X_{CO} with a higher H_2O/CO ratio is less pronounced for the 2D heterogeneous model, as it accounts for dispersive phenomena that further limit reactant conversion. In practice, increasing the water concentration in the reaction medium helps prevent carbon deposition on the catalyst (Sanz *et al.*, 2015).

Figure 3 illustrates that an increase in transmembrane pressure enhances X_{CO}. Pressure serves as the driving force for hydrogen permeation through the membrane, and its increase results in a higher H_2 permeation flow, facilitating the equilibrium shift toward product formation and accelerating reactant consumption. Additionally, higher pressure enhances the reaction rate by increasing the scale-up factor (F_{press}) (El Bazi *et al.*, 2022) and the concentrations of H_2O and CO.

Given its satisfactory agreement with experimental data, the rigorous 1D heterogeneous approach is adopted for the remainder of this study.

3.2. Impact of Catalyst Particle Geometric Characteristics on Membrane Reactor Behavior

Figures 4a, 4b, and 4c illustrate the effect of catalyst geometric characteristics (shape, volume) on catalyst effectiveness factor, P_{H_2}, X_{CO}, and temperature (T) along the membrane reactor. This section of the study considers the feed flow rate, molar composition, catalyst properties, reactor and membrane characteristics, feed temperature, transmembrane pressure, and permeate conditions, as presented in Table 1. The heat transfer mode of the membrane reactor is also provided in Table 1, assuming no sweep gas is used.

The results in Figure 4.a examine two catalyst geometries (cylindrical and spherical) with a particle volume of 169.5 mm^3. This figure is characterized by a rise in P_{H2} at the upstream positions of the reactor, followed by a decrease in this parameter throughout the rest of the converter. At the reactor inlet, high reactant concentrations lead to a high reaction rate (Eq. 7) and enhanced hydrogen production, causing an increase in hydrogen partial pressure. As the reaction progresses, reactant concentrations decrease while product concentrations increase, which reduces the reaction rate (Eq. 7). Meanwhile, the increasing P_{H2} enhances hydrogen permeation through the membrane (Eq. 13). In the more advanced positions of the reactor, more hydrogen is removed through the membrane than is produced by the WGS reaction, resulting in a decline in P_{H2}. A similar P_{H2} profile was reported in the study by Adrover *et al.* (2017). According to the same figure, spherical particles exhibit the highest effectiveness factor. This is because the spherical shape provides a larger surface area exposed to the surrounding fluid (A_p in m^2), enhancing contact with the reaction medium compared to the cylindrical shape. As a result, diffusional resistance is greater for cylindrical particles. This occurs

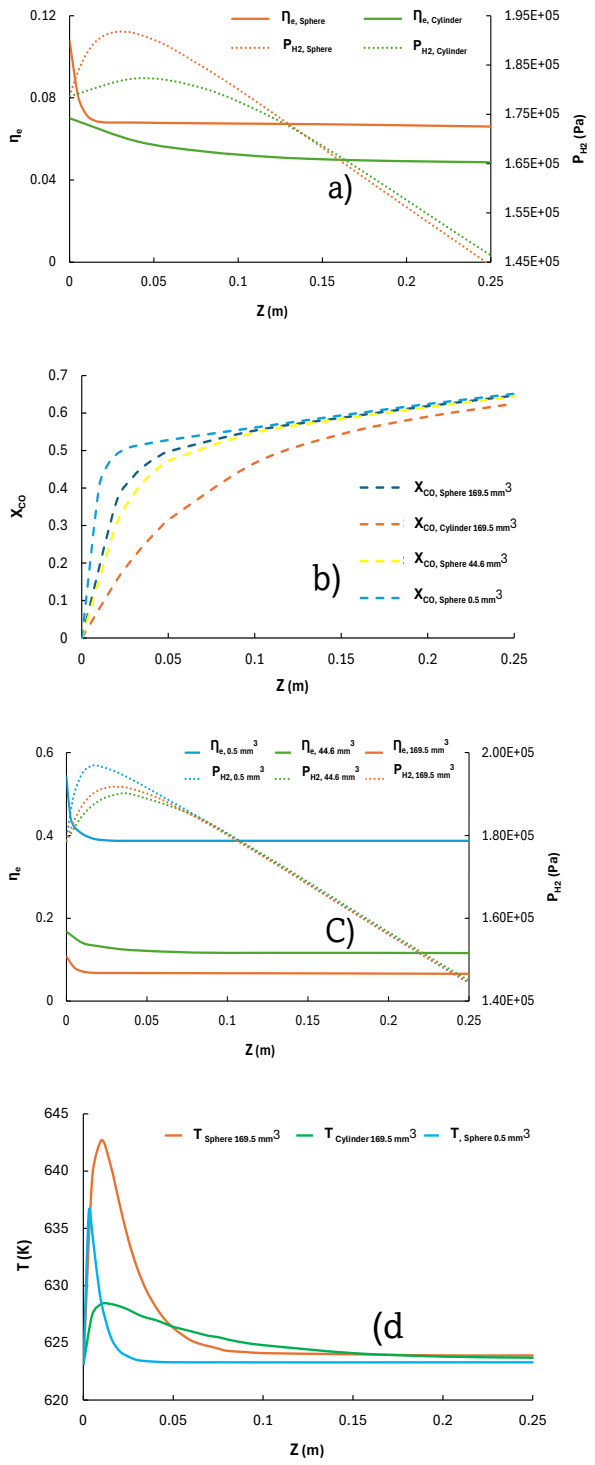

Fig. 4 Effect of particle geometry on membrane reactor performance: (a) Particle shape influence on P_{H_2} and η_e, (b) shape and size effects on X_{CO}, (c) volume impact on P_{H_2} and η_e, and (d) shape and volume effects on temperature Profile

because the effective diffusional path length ($l_C = \frac{V_p}{A_p}$) is longer for geometries with a smaller surface area exposed to the fluid (Mandic *et al.*, 2017). The consequence of this higher effectiveness factor in spherical grains is greater reaction activity at the reactor inlet, resulting in a higher CO conversion for this geometry (Figure 4.b) and leading to higher hydrogen productivity. Due to their higher effectiveness factor, spherical particles exhibit greater reaction activity at the reactor inlet, leading to higher CO conversion (Figure 4.b) and increased hydrogen productivity. Consequently, the retentate P_{H2} is higher at the reactor inlet for this geometry (Figure 4.a). However, the increase in H_2 concentration inside the reactor also slows down the reaction rate in the rest of the reactor (Eq. 7). As a result, despite the superior effectiveness factors of spherical particles, simulations did not reveal significant differences in X_{CO} at the reactor outlet. Specifically, X_{CO} is 0.64 for spherical particles and 0.62 for cylindrical particles (Figure 4.b). It is also noted that from Z = 0.12 m onward, the P_{H2} profiles for both shapes become very similar (Figure 4.a). This convergence in P_{H_2} profiles throughout the rest of the reactor results in similar hydrogen permeation flow rates ($F_{h2,p}$) for both shapes (Eqs. 6, 13). The simulations indicate that $F_{h2,p}$ is 2.1×10^{-4} mol·s^{-1} for spheres and 2.026×10^{-4} mol·s^{-1} for cylinders. Figure 4.c explores the effect of three different particle volumes (0.5 mm³, 44.6 mm³, and 169.5 mm³) for a spherical geometry. The results clearly show that smaller particles exhibit a higher effectiveness factor due to reduced intragranular diffusion limitations (Mandic *et al.*, 2017; Wang *et al.*, 2001; Zhang *et al.*, 2014). This enhancement in catalyst effectiveness factor for smaller particles increases reaction activity, leading to higher CO conversion at the reactor inlet for the smallest particle volume (0.5 mm³, Figure 4.b) and greater hydrogen productivity in regions closer to the converter inlet, as indicated by higher P_{H2} values in the retentate for these positions. However, as previously observed, the rise in H_2 concentration inside the reactor slows down the reaction rate. Consequently, despite the superior effectiveness factor of smaller particles, simulations did not reveal significant differences in X_{CO} at the reactor outlet ($X_{CO} \approx 0.65$ for all three particle sizes studied), which is consistent with the results of Marin *et al.* (2012), nor in P_{H_2} profiles at advanced positions along the reactor. From Z=0.06 m onward, the P_{H2} profiles overlap for all three volumes (Figure 4.c). This overlap results in similar hydrogen permeation flow rates, approximately 2.1×10^{-4} mol. s^{-1} for all three particle sizes.

The analysis of the effect of particle shape on the temperature profile inside the reactor (Figure 4.d) shows that the temperature increase at the reactor inlet is more pronounced for a reactor packed with spherical particles compared to one filled with cylindrical particles of the same volume. This can be attributed to the higher effectiveness factor of the spherical shape, which leads to an increased reaction rate at the reactor inlet and, consequently, greater heat release from the chemical reaction. Furthermore, simulations indicate that the individual heat transfer coefficient on the reactor side (h_{int}) is lower for the 169.5 mm³ spherical particles than for the cylindrical particles of the same volume ($h_{int} \in$ [30–38.6] W·m^{-2}·K^{-1} for spheres and $h_{int} \in$ [48.5–59] W·m^{-2}·K^{-1} for cylinders). These lower heat transfer coefficients limit heat dissipation toward the shell in the membrane reactor packed with spherical particles.

Comparing the temperature profile of a reactor packed with spherical catalyst particles (previously discussed) to that of a reactor packed with smaller spherical particles (0.5 mm³, Figure 4.d) reveals that the temperature rise at the reactor inlet is less pronounced for the latter. Although smaller particles exhibit higher effectiveness factors—resulting in increased reaction rates and, consequently, greater heat release at the reactor inlet—they also enhance heat dissipation toward the shell. Simulations indicate that the individual heat transfer coefficient (hi_{nt}) for these smaller particles ranges from 133.1 to 177.6 W·m^{-2}·K^{-1}, which is significantly higher than that observed for the reactor packed with 169.5 mm³ spherical particles. This

result may be attributed to the smaller particle diameters and the lower bed porosity in reactors packed with finer particles.

Results obtained using Equation (9) indicate that particle shape has no significant impact on pressure drop, which remains almost negligible under the studied conditions for a particle volume of 169.5 mm³. However, a pressure drop of 0.0964% is observed for small spherical particles of 0.5 mm³. Although this pressure drop is minimal under the examined conditions, the impact of small particle size on pressure loss is expected to be more significant in industrial-scale reactors.

3.3. Effect of Sweep Gas Flow Rate on Reactor Behavior

Figures 5.a, 5.b, and 5.c illustrate the evolution of the hydrogen permeation flux (J_{H_2}), carbon monoxide conversion, reaction rate, hydrogen pressure in the retentate, and temperature along the membrane reactor for different sweep gas flow rates, as presented in Table 1. The operating conditions, membrane reactor characteristics, and catalyst properties are also listed in this Table. The catalyst particles are assumed to be spherical, with a volume of 169.5 mm³.

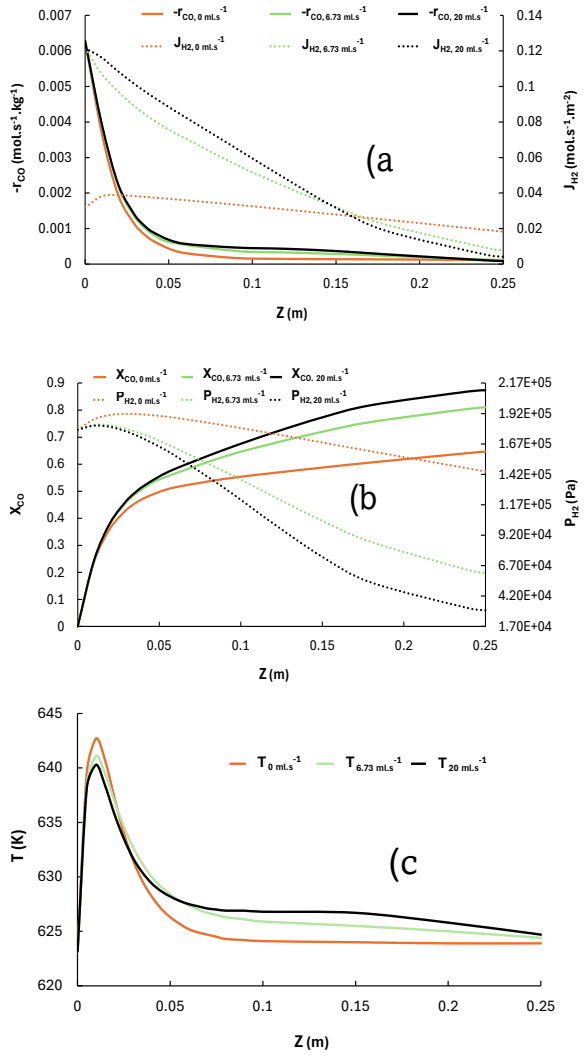

Fig. 5 Effect of sweep gas flow rate on membrane reactor performance: (a) Impact on reaction rate ($-r_{CO}$) and hydrogen permeation flux (J_{H_2}), (b) Effect on CO conversion (X_{CO}) and hydrogen partial pressure (P_{H_2}), (c) Influence on temperature profile

An increase in the sweep gas flow rate leads to a higher J_{H_2}, which is in agreement with the literature (Eddi & Chibane, 2020). This is because a greater sweep gas flow inside the inner tube dilutes the hydrogen in this region, thereby reducing P_{H_2p}. Consequently, the hydrogen permeation flow increases (Eq. 14), as shown in Figure 5.a. The increase in hydrogen evacuation toward the permeate side with the rise in sweep gas flow rate leads to a decrease in hydrogen concentration in the retentate, which is reflected by a reduction in P_{H_2} as the sweep gas flow rate increases (Figure 5.b). The decrease in hydrogen pressure in the retentate results in a lower H_2 concentration in the reactor. This, in turn, enhances the reaction rate as the sweep gas flow increases (Eq. 7), as observed in Figure 5.a.

Figure 5.b also highlights the positive effect of the sweep gas flow rate on reactant conversion, with X_{CO} increasing from 0.65 in the absence of sweep gas to 0.87 for an N_2 flow rate of 20 ml·s^{-1}, confirming previous observations in the literature (Abdel-Hamid *et al.*, 2018; Boutikos & Nikolakis, 2010; Chein *et al.*, 2014). This result is attributed to the increase in reaction rate caused by the reduction in P_{H_2} induced by the sweep gas (Figure 5.a). The rise in hydrogen permeation flow leads to an increase in $F_{H_2,p}$. Simulations indicate that $F_{H_2,p}$ increases from 2.1 × 10^{-4} mol·s^{-1} in the absence of sweep gas to 3.315× 10^{-4} mol·s^{-1} at a sweep gas flow rate of 6.73 ml·s^{-1}, and further to 3.575 × 10^{-4} mol·s^{-1} when the sweep gas flow rate reaches 20 ml·s^{-1}. A similar effect of the sweep gas has been observed in methane reforming membrane reactors (Coronel *et al.*, 2011). Figure 5.c reveals a slight influence of the sweep gas flow rate on the temperature profile inside the reactor. Due to the cooling effect of the sweep gas, the maximum temperature in the membrane reactor decreases from 642.7 K in its absence to 640.3 K at a sweep gas flow rate of 20 ml·s^{-1}. Finally, simulations do not indicate any significant effect of the sweep gas flow rate on the pressure drop inside the membrane reactor.

3.4. Comparison of the Conventional Fixed-Bed Reactor and the Membrane Reactor

Figures 6.a and 6.b compare the performance of a membrane reactor and a conventional fixed-bed reactor in terms of effectiveness factor, hydrogen pressure in the converter, carbon monoxide conversion, and reaction rate. The operating conditions, heat transfer mode, and characteristics of both the membrane reactor and the catalyst are summarized in Table 1. The catalyst particles are assumed to be spherical with a volume of 169.5 mm³, and the process is considered to operate without a sweep gas. As shown in Figure 6.a, the presence of the membrane has no significant impact on the catalyst, as the effectiveness factor profiles along the reactor are nearly identical for both processes. However, the hydrogen pressure profile in the retentate along the membrane reactor differs from that of the conventional fixed-bed reactor.

In the membrane reactor, the partial pressure of hydrogen (P_{H_2}) increases from 1.79 × 10^5 Pa at Z = 0 m to 1.92 × 10^5 Pa at Z = 0.03 m, before decreasing along the reactor length, reaching 1.444 × 10^5 Pa at Z = 0.25 m. Although hydrogen is produced via the chemical reaction, its continuous permeation across the membrane results in a progressive decline in P_{H_2}. In contrast, in the conventional fixed-bed reactor, P_{H_2} increases from 1.79 × 10^5 Pa at Z = 0 m to 2.004 × 10^5 Pa at Z = 0.09 m, beyond which it remains approximately constant. This stabilization of hydrogen pressure at Z = 0.09 m suggests that equilibrium is attained at this position.

The ability of the membrane reactor to continuously evacuate hydrogen leads to higher reaction rates (Figure 6.b), as the reduction in hydrogen concentration enhances the

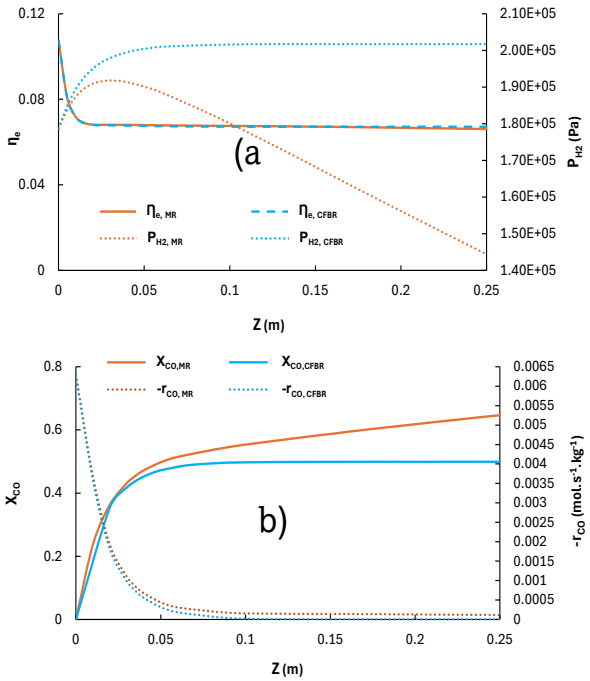

Fig. 6. Comparison Between the Membrane Reactor and the Conventional Fixed-Bed Reactor: (a) η_e and PH_2 Profiles, (b) XCO and −rCO Profiles for Both Configurations

reaction kinetics (Eq. 7). Moreover, unlike the conventional fixed-bed reactor, where the reaction rate approaches zero at the equilibrium position (Z = 0.09 m), the membrane reactor shifts the equilibrium, maintaining a nonzero reaction rate throughout the reactor.

The higher reaction rates ($-r_{CO}$) in the membrane reactor result in greater X_{CO} values compared to the conventional reactor (Figure 6.b). This finding is consistent with the literature (Abdel-Hamid *et al.*, 2018; Adrover., 2009b; Meng *et al.*, 2021). In fact, in the conventional reactor, X_{CO} increases from 0 to approximately 0.5 between the reactor inlet and the equilibrium position (Z = 0.09 m), remaining constant thereafter. In contrast, in the membrane reactor, carbon monoxide conversion continues to increase along the reactor length, reaching approximately 0.65 at the outlet.

The heat released by the reaction in the upstream region (Z ≤ 0.03 m), where reaction rates are highest, and the cooling imposed by the shell determines the temperature profile in the process. Since these factors are nearly identical in both reactors, simulations did not reveal any significant differences in temperature profiles between the membrane reactor (MR) and the conventional fixed-bed reactor(CFBR). Finally, the simulations did not show any significant pressure drops along the conventional fixed-bed reactor.

4. Conclusion

In this study, dedicated to developing an approach for predicting the behavior of a small-scale WGS membrane reactor, we demonstrated that the rigorous 1D heterogeneous model provides more accurate predictions of experimental data from the literature—obtained under various operating conditions (GHSV, temperature, H_2O/CO ratio, transmembrane pressure)—compared to the 1D pseudo-homogeneous model, which remains the most widely used in many published studies. Moreover, our analysis underscored the significant influence of the catalytic particle's geometric characteristics on the catalyst's effectiveness factor and on key parameters at the reactor inlet, including CO conversion, H_2 pressure in the retentate, and temperature profile. However, we observed that these effects are less pronounced at the outlet of the studied membrane reactor.

The simulations further demonstrated that using a sweep gas flow rate of 20 mL·s^{-1} enhances the permeation flow of hydrogen by 58% and increases carbon monoxide conversion by 34%. Lastly, the comparison between the studied membrane reactor and a conventional fixed-bed reactor revealed that the membrane has no significant impact on the effectiveness factor, while CO conversion in the membrane reactor is approximately 30% higher.

The scale-up from laboratory to industrial applications requires the adopting of a 2D model to account for dispersive phenomena, which are more pronounced in membrane reactors. Our future work will focus on extending the rigorous heterogeneous approach developed in this study to a 2D model for the investigation of industrial WGS membrane reactors.

Author Contributions: W. El Bazi: Conceptualization, Methodology, Software, Supervision; W. El Bazi, A. Abidi, S. Yadir and B. Messnaoui: Formal Analysis, Invistigation, Ressources, Commentary or revision; W. El Bazi, and A. Abidi: Writing - Review & Editing. All authors have read and agreed to the published version of the manuscript. Analysis, Invistigation, Ressources, Commentary or revision; W. El Bazi, and A. Abidi: Writing - Review & Editing. All authors have read and agreed to the published version of the manuscript.

Funding: None.

Conflicts of Interest: The authors declare no conflict of interest.

References

Abdel-Hamid, A., Mourad,I., Ghasem, M.N., & Alraeesi, A.Y. (2018). Modelling and Simulation of Hydrogen Production via Water Gas Shift Membrane Reactor. *International Journal of Chemical Engineering and Applications*, 9(4), 112-118. https://doi.org/10.18178/ijcea.2018.9.4.709

Adrover, M.E., López, E., Borio, D.O., & Pedernera, M.N. (2009a). Simulation of a membrane reactor for the WGS reaction: Pressure and thermal effects. *Chemical Engineering Journal, 154(1-3), 196-202.* https://doi.org/10.1016/j.cej.2009.04.057

Adrover, M.E., Lopez, E., Borio, D.O., & Pedernera, M.N. (2009b). Theoretical Study of a Membrane Reactor for the Water Gas Shift Reaction Under nonisothermal Conditions. *AIChE Journal*, 55 (12), 3206-3213. https://doi.org/10.1002/aic.11929

Adrover, M.E., Borio, D., & Pedernera, M. (2017). Comparison between WGS membrane reactors operating with and without sweep gas: Limiting conditions for co-current flow. *International Journal of Hydrogen Energy*, 42(8), 5139-5149. https://doi.org/10.1016/j.ijhydene.2016.11.075

Alihellal, D., & Chibane, L. (2016a). Simulation study of the effect of water removal from Fischer–Tropsch products on the process performance using a hydrophilic membrane reactor. *Reaction Kinetics, Mechanisms and Catalysis*, 117, 605-621. https://doi.org/10.1007/s11144-015-0961-x

Alihellal, D., & Chibane, L. (2016b). Comparative Study of the Performance of Fischer–Tropsch Synthesis in Conventional Packed Bed and in Membrane Reactor Over Iron- and Cobalt-Based Catalysts. Arabian Journal for Science and Engineering, 41, 357-369. https://doi.org/10.1007/s13369-015-1836-1

Alihellal, D., & Chibane, L. (2019). Modeling and simulation of the water gas shift reaction for the hydrogen production in two membrane reactors, , *First International Workshop On Environmental Engineering*, Setif- Algeria (2019).

Alihellal, D., Hadjam, S., & Chibane, L. (2024). Mathematical modeling and evaluation of permeation and membrane separation performance for Fischer–Tropsch products in a hydrophilic membrane reactor. *Chemical Product and Process Modeling*, 19(3), 433-446. https://doi.org/10.1515/cppm-2023-0016

Augustine, A.S., Ma, Y.H., & Kazantzis, N.K. (2011). High pessure palladium membrane reactor for the high temperature water gas shift reaction. *International Journal of Hydrogen Energy,* 36 (9), 5350-5360. https://doi.org/10.1016/j.ijhydene.2011.01.172

Basile, A., Curcio, S., Bagnato, G., Liguori, S., Jokar, S.M., & Iulianelli, A. (2015). Water gas shift reaction in membrane reactors: Theoretical investigation by artificial neural networks model and experimental validation. *International Journal of Hydrogen Energy,* 40(17), 5897-5906. https://doi.org/10.1016/j.ijhydene.2015.03.039

Bishop, B.A., & Lima, F.V. (2020). Modeling, Simulation, and Operability Analysis of a Nonisothermal, Countercurrent, Polymer Membrane Reactor. *Processes,* 8(1), 78. https://doi.org/10.3390/pr8010078

Boutikos, P., & Nikolakis, V. (2010). A simulation study of the effect of operating and design parameters on the performance of a water gas shift membrane reactor. *Journal of Membrane Science*, 350(1-2), 378-386. https://doi.org/10.1016/j.memsci.2010.01.014

Brunetti, A., Caravella, A., Barbieri, G., & Drioli, E. (2007). Simulation study of water gas shift reaction in a membrane reactor. *Journal of Membrane Science,* 306(1-2), 329-340. https://doi.org/10.1016/j.memsci.2007.09.009

Coronel, L., Múnera, J.F., Lombardo, E.A., & Cornaglia, L.M. (2011). Pd based membrane reactor for ultra-pure hydrogen production through the dry reforming of methane. Experimental and modeling studies. *Applied Catalysis A: General*, 400(1-2), 185-194. https://doi.org/10.1016/j.apcata.2011.04.030

Chein, R.Y., Chen, Y.C., Chyou, Y.P., & Chung, J.N. (2014). Three-dimensional numerical modeling on high pressure membrane reactors for high temperature water-gas shift reaction. *International Journal of Hydrogen Energy*, 39(28), 15517-15529. https://doi.org/10.1016/j.ijhydene.2014.07.113

Eddi, I., & Chibane, L. (2020). Performance assessment of high temperature water-gas-shift reaction for hydrogen generation and its purification in a membrane reactor/separator of hydrogen or of carbon dioxide. Chemical Product and Process Modeling,16(4), 261-280. https://doi.org/10.1515/cppm-2019-0134

El Bazi, W., Bideq, M., El Abidi, A., Yadir, S., & Ouartassi, B. (2022). Numerical Study of a Water Gas Shift Fixed Bed Reactor Operating at Low Pressures. *Bulletin of Chemical Engineering Reaction and Catalysis*, 17(2), 304-321. https://doi.org/10.9767/bcrec.17.2.13510.304-321

El Bazi, W., Bideq, M., Yadir, S., & El Abidi, A. (2023). Efects of catalyst distribution, particle geometry, and process conditions on the behavior of a water gas shift reactor under moderate pressures: a modeling study. *Reaction Kinetics, Mechanisms and Catalysis*, 136, 1859-1890. https://doi.org/10.1007/s11144-023-02431-x

Gao, W., Zhou, T., Gao, Y., & Wang, Q. (2019). Enhanced water gas shift processes for carbon dioxide capture and hydrogen production. *Applied Energy*. 254, 113700. https://doi.org/10.1016/j.apenergy.2019.113700

Garshasbi, A., Chen, H., Cao, M., Karagöz, S., Ciora, Jr R.J., Liu, P.K.T., Manousiouthakis ,V.I., & Tsotsis, T.T. (2019). Membrane-based reactive separations for process intensification during power generation. *Catalysis Today* ,331, 18–29. https://doi.org/10.1016/j.cattod.2017.10.039

Gosiewski, K., Warmuzinski, K., & Tanczyk, M. (2010). Mathematical simulation of WGS membrane reactor for gas from coal gasification. *Catalysis Today*, 156(3-4), 229-236. https://doi.org/10.1016/j.cattod.2010.02.031

Huang, J., El-Azzami, L., & Winston Ho, W.S. (2005). Modeling of CO_2-selective water gas shift membrane reactor for fuel cell. *Journal of Membrane Science*, 261(1-2), 67-75. https://doi.org/10.1016/j.memsci.2005.03.033

Huang, H., Samsun,R.C., Peters, R., & Stolten, D. (2022). CFD modeling of a membrane reactor concept for integrated CO_2 capture and conversion. *React. Chem. Eng*, 7(12), 2573-258. https://doi.org/10.1039/D2RE00282E

Israni, S.H., & Harold, M.P. (2011). Methanol steam reforming in single-fiber packed bed Pd–Ag membrane reactor: Experiments and modeling. *Journal of Membrane Science*, 369(1-2), 375-387. https://doi.org/10.1016/j.memsci.2010.12.029

Karagoz, S., Cruz, F.E.D., Tsotsis, T.T., & Manousiouthakis, V.I. (2018). Multi-Scale Membrane Reactor (MR) modeling and Simulation for the Water Gas Shift Reaction. *Chemical Engineering and Processing - Process Intensification*, 133, 245-262. https://doi.org/10.1016/j.cep.2018.09.012

Karagoz, S., Tsotsis, T.T., & Manousiouthakis, V.I. (2020). Multi-scale model based design of membrane reactor/separator processes for intensified hydrogen production through the water gas shift reaction. *International Journal of Hydrogen Energy,* 45(12), 7339-7353. https://doi.org/10.1016/j.ijhydene.2019.05.118

Keiski, R.L., Desponds,O ., Chang, Y-F., & Somorjai, G.A. (1993). Kinetics of the water-gas shift reaction over several alkane activation and water-gas shift catalysts. *Applied Catalysis A: General.* 101(2), 317-338. https://doi.org/10.1016/0926-860X(93)80277-W

Lundin, S-T. B., Miklautz, M., Ikeda, A., Hasegawa, Y., & Oyama, S.T. (2023). Criteria for the use of 1D and 2D models in catalytic membrane reactor modeling. *Chemical Engineering Journal*, 477, 147007. https://doi.org/10.1016/j.cej.2023.147007

Ma, D., & Lund, C.R.F. (2003). Assessing High-Temperature Water-Gas Shift Membrane Reactors. *Ind. Eng. Chem. Res*, 42(4), 711–717. https://doi.org/10.1021/ie020679a

Makertiharta,I G B N., Rizki, Z., Zunita, M., & Dharmawijay, P.T. (2017). Simulation of Water Gas Shift Zeolite Membrane Reactor. *IOP Conf. Ser.: Mater. Sci. Eng,* 214 012013. https://doi.org/10.1088/1757-899X/214/1/012013

Mandic, M., Branislav, T., Zivanic, L., Nikacevic, N., & Bukur, DB. (2017). Efects of catalyst activity, particle size and shape, and process conditions on catalyst efectiveness and methane selectivity for Fischer–Tropsch reaction: a modeling study. *Ind Eng Chem Res*, 56(10), 2733–2745. https://doi.org/10.1021/acs.iecr.7b00053

Marin, P., Diez, F.V., & Ordonez, S. (2012). Fixed bed membrane reactors for WGSR-based hydrogen production: Optimisation of modelling approaches and reactor performance. *International Journal of Hydrogen Energy*, 37(6), 4997-5010. https://doi.org/10.1016/j.ijhydene.2011.12.027

Markatos, N.C., Vogiatzis, E., Koukou, M.K., & Papayannakos, N. (2005). Membrane Reactor Modelling : A Comparative Study to Evaluate the Role of Combined Mass and Heat Dispersion in Large-scale Adiabatic Membrane Modules. *Chemical Engineering Research and Design*, 83(10), 1171-1178. https://doi.org/10.1205/cherd.04299

Mendes, D., S, Sa., Tosti, S., Sousa, J.M., Madeira, L.M., & Mendes, A. (2011). Experimental and modeling studies on the low-temperature water-gas shift reaction in a dense Pd–Ag packed-bed membrane reactor. *Chemical Engineering Science*, 66(11), 2356-2367. https://doi.org/10.1016/j.ces.2011.02.035

Meng, L., Ovale Encinia, O., & Lin, J.Y.S. (2021). Catalyst-Free Ceramic-Carbonate Dual-Phase Membrane Reactors for High-Temperature Water Gas Shift: A Simulation Study. *Ind. Eng. Chem. Res,* 60(9), 3581–3588. https://doi.org/10.1021/acs.iecr.1c00541

Olatunji, S.O., & Camacho, L.M. (2018). Heat and Mass Transport in Modeling Membrane Distillation Configurations: A Review. *Frontiers in Energy Research,* 6, 1-18. https://doi.org/10.3389/fenrg.2018.00130

Oyama, S.T., & Hacarlioglu, P. (2009). The boundary between simple and complex descriptions of membrane reactors: The transition between 1-D and 2-D analysis. *Journal of Membrane Science*, 337(1-2), 188-199. https://doi.org/10.1016/j.memsci.2009.03.040

Piemonte, V., De Falco, M., & Basile, A. (2015). Performance Assessment of Water Gas Shift Membrane Reactors by a Two-dimensional Model. *Energy Sources, Part A: Recovery, Utilization, and environmental effects,* 37(20), 2174-2182. https://doi.org/10.1080/15567036.2012.691945

Radcliffe, A.J., Singh, R.P., Berchtold, K.A., & Lima, V.F. (2016). Modeling and Optimization of High-Performance Polymer Membrane Reactor Systems for Water–Gas Shift Reaction Applications. *Processes,* 4(2), 8. https://doi.org/10.3390/pr4020008

Sanz, R., Calles, J.A., Ordóñez, S., Marín, P., Alique, D., & Furones, L. (2013). Modelling and simulation of permeation behaviour on Pd/PSS composite membranes prepared by “pore-plating” method. *Journal of Membrane Science*, 446, 410-421. https://doi.org/10.1016/j.memsci.2013.06.060

Sanz, R., Calles, J.A., Alique, D., & Furones, L. (2014). H_2 production via water gas shift in a composite Pd membrane reactor prepared by the pore-plating method. *International Journal of Hydrogen Energy*, 39(9), 4739-4748. https://doi.org/10.1016/j.ijhydene.2013.12.145

Sanz, R., Calles, J.A., Alique, D., Furones, L., Ordonez, S., & Marın, P. (2015). Hydrogen production in a Pore-Plated Pd-membrane reactor. :Experimental analysis and model validation for the Water Gas Shift reaction. *International Journal of Hydrogen Energy*, 40(8), 3472-3484. https://doi.org/10.1016/j.ijhydene.2014.11.120

Smith, R.J.B., Loganathan, M., & Shantha, M.S. (2011). CFD Simulation of Water Gas Shift Membrane Reactor—Pressure Effects on the Performance of the Reactor. *Chemical Product and Process Modeling*, 6(1), Article 33. https://doi.org/10.2202/1934-2659.1595

Villermaux, J. (1993) Génie de la réaction chimique, *2nd edn. Tec & Doc*, Paris.

Wang, Y-N., Xu, Y-Y., Xiang, H-W., Li, Y-W., & Zhang, B-J. (2001). Modeling of catalyst pellets for Fischer–Tropsch synthesis. *Ind Eng Chem Res*, 40(20), 4324–4335. https://doi.org/10.1021/ie010080v

Wirawan, S.K., Creaser, D., Bendiyasa, I.M., & Sediawan, W.B. (2012). CO_2 Selective Water Gas Shift Membrane Reactor : Modeling and Simulation. *AJCHE*, 12(1), 59-72. https://doi.org/10.22146/ajche.49756

Zhang, L., Zhang, HT., Ying, WY., & Fang ,DY. (2014). The simulation of an industrial fxed bed reactor for methanol dehydration to dimethyl ether. *Energy Sources A*, 36(19), 2166–2174. https://doi.org/10.1080/15567036.2012.750404